

Franc Kosel · Jože Petrišič · Boris Kuselj
Tadej Kosel · Viktor Šajn · Mihael Brojan

Local buckling and debonding problem of a bonded two-layer plate

Received: 8 July 2003 / Accepted: 9 February 2005 / Published online: 28 July 2005
© Springer-Verlag 2005

Abstract The problem of local buckling, debonding initiation and growth process of the debonding of a bonded two-layer plate is treated. In the weaker layer of the plate, compression appears due to the external compressive axial force and bending moment. The conditions for local buckling of the weaker layer have been studied where the possibility that the stress state in the layers could be in elasto-plastic domain has been considered. A mathematical model is developed to determine the bending displacements of laminate layers after the weaker layer buckles locally, and in the state after the plate has been unloaded. The third-order theory introduced by Chwalla has been implemented. Mechanical properties of the layers and adhesive used in the numerical model were measured with experiments. Experimental work comprised the determination of mechanical properties of the chosen materials and experimental verification of the presented mathematical model. Numerically obtained results are compared with those obtained by an experimental approach, and are found to be in good agreement.

Keywords Local buckling · Debonding growth process · Loading process · Unloading process · Experimental verification

List of symbols

i	Subscript denoting the number of layers
L, U, R	Subscript denoting loading, unloading and state after unloading
A_i	Cross section of a layer
b	Width of plate
E_i	Young's modulus in the elastic domain
E_{ti}	Tangent modulus in the plastic domain
h_i	Thickness of layer
h_N	Internal height of debonded area
h_Z	External height of debonded area
$M_i(x)$	Internal bending moment
$n.a.$	Neutral axis of layer
$N_i(x)$	Internal axial force
$Q_i(x)$	Internal shear force
$v_i(x)$	Bending displacement of layer
$y_{Ni}(x)$	Position of neutral axis
$\alpha_i(x)$	Angle of inclination

$\Delta y_{Ni}(x)$	Distance between the centroid and the neutral axis
$\kappa_i(x)$	Curvature of layer
$\sigma_q(\epsilon_q)$	Tensile stress in adhesive
$\sigma_{xi}(x)$	Stress in layer
σ_y	Yield stress

1 Introduction

Through-width delamination [1] is a defect of multilayer plates that can appear due to various reasons. It may be caused by external bending moment, external compressive axial force or both of them acting at the same time on parallel edges of a laminate (Fig. 1). Initial defects in laminates and bonded multilayer plates occur in domains between layers where adhesion is imperfect. These domains are very sensitive to layer local buckling.

Extensive research of delamination in plates caused by local buckling due to external compressive forces began in the late 1970s [2]. Numerous analytical and numerical models have been developed and solved mainly by the finite element method (FEM), as reported in [3–6]. In the early 1990s, a number of research studies focused on the bearing strength of the plates in the postbuckled state [2, 6]. The postbuckled state is the deformed state into which a plate enters after the external load has exceeded its critical value. Initial defects, especially in bonded multilayer plates, can show up in one or more debonded areas with decreased adhesion or loss of adhesion in the adhesive between the layers. Some researchers have also studied and analyzed conditions under which local buckling could occur in the laminates without initial defects, as reported in [7] and [8]. Their work shows that certain combinations of external compressive or bending loads and bonding material quality may lead to local buckling even if no initial defects are present. However normally it would occur due to the presence of an initial defect in the bonding material.

The main goal of our research was to develop and experimentally verify a suitable mathematical model for the definition of mechanical, geometrical and material parameters at which the weaker layer of a bonded two-layer plate can buckle locally if the plate is loaded by external compressive force and bending moment. An evaluation is made of the growth of the debonded area and the bending displacement states of the layers when the external bending moment is growing due to a constant compressive force, and in the state after unloading.

2 Formulation of the problem

An ideally flat, bonded two-layer plate with the rigidity of layer 1 much bigger than that of layer 2 is chosen for the discussion (Fig. 2). The plate is chosen so that it is rigidly fixed at point T. It is assumed that at the beginning of loading the layers are bonded along their entire length with an adhesive having a certain stress–strain relation defined by the function $\sigma_q = \sigma_q(\epsilon_q)$. The thickness of the adhesive layer is much smaller than that of the metal layers, and can therefore be neglected. The plate is loaded with external compressive axial force F_0 and bending moment M_0 (Fig. 2). In the weaker layer 2, internal compressive force appears due to the chosen direction of the moment M_0 . At certain loads, mechanical properties and geometry of the plate, layer 1 bends whereas layer 2 buckles locally into a shape with minimal potential energy. Due to the symmetrical supports and loads the deformed shape of the plate is symmetrical, only half of the plate can be treated.

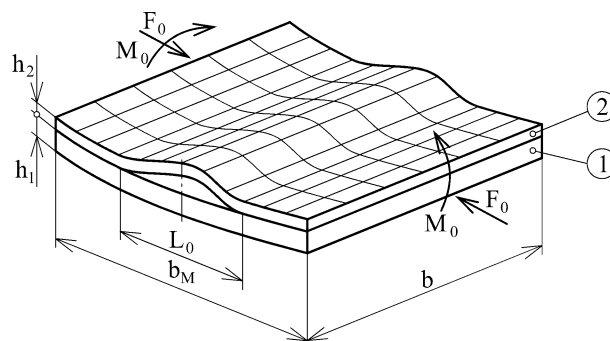


Fig. 1 Through-width delamination

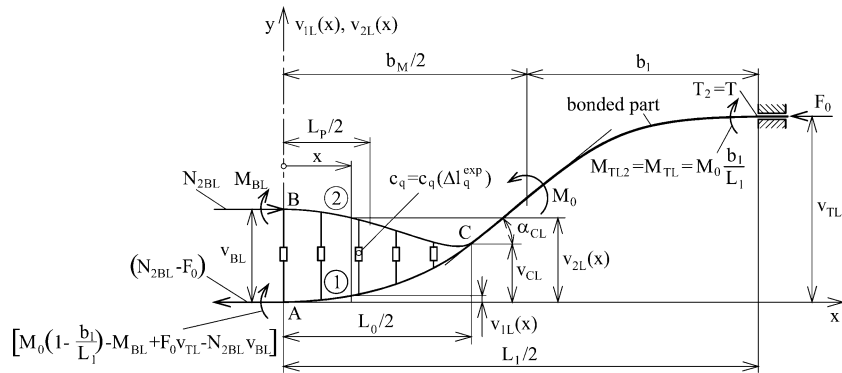


Fig. 2 The right-hand part of plate

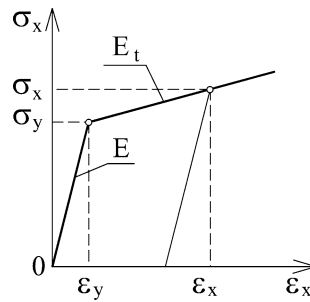


Fig. 3 Stress–strain relationships of layers 1 and 2

The loading model is chosen so that 90% of the compressive force that should induce local buckling of layer 2 is performed by the force F_0 while the remaining part is the bending moment M_0 . The geometry of the plate is chosen so that the local buckling of the weaker layer could take place in the elasto–plastic domain of both layers. Layers are made of materials having an elastic, linear strain-hardening stress–strain relation (Fig. 3).

Thus the stress in the plastic domain can be defined by the expression:

$$\sigma_x = \sigma_y + E_t(\varepsilon_x - \varepsilon_y), \quad (1)$$

where ε_y is the strain at the yield stress.

The process of debonding of the plate in the postbuckled state is observed at a constant external compressive force F_0 and increasing bending moment M_0 .

3 Mathematical model for the determination of the bending displacements and stress states in the plate

We will divide the process of debonding into three different physical phases. In the first phase, considering the second-order theory [9], we will determine the bending displacement state of the layers in the moment right after local buckling of layer 2, the force, and the critical external bending moment at which the unstable state in layer 2 occurs. This state will be called state “0”. In the second phase, the plate is in the postbuckled state, here called state “1”. In this phase, considering the exact expression for the curvatures of the layers during the increasing external loads, we will determine stresses and bending displacement states of the plate. We will analyze the conditions for growth of the debonded area. In the third phase, the bending displacement state of the plate after unloading will be obtained.

3.1 Bending displacements in the moment right after local buckling of layer 2—Phase 1

Since in the postbuckled state the plate is symmetrical with respect to the y -axis, the tangents to both layers at points A and B are parallel to x -axis (Fig. 2). The equilibrium states of the internal forces and internal bending

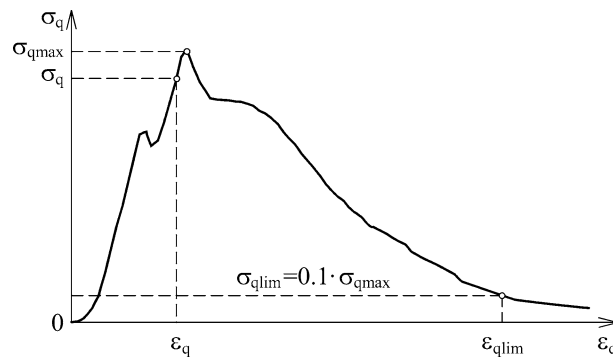


Fig. 4 Measured stress–strain relationship of the adhesive

moments are analyzed on small elements, which are cut from the plate in its deformed state. It is assumed that, prior to loading, the plate is ideally flat. Therefore the bending displacements of the layers right after buckling of layer 2 are very small. Thus, for the determination of the bending displacements in this indifferent state, we can use the theory of small bending displacements, according to which the radius of curvature is defined by a simplified equation $\rho^{-1}(x) = \frac{d^2v(x)}{dx^2} = v''(x)$.

In the mathematical model for the determination of the bending displacements of the layers, we consider the actual rheological model of the adhesive. The strain of the bonded joint is defined by equation $\varepsilon_q(x) = \Delta l_q^{\text{exp}}(x)/\bar{h}_A$, where $\Delta l_q^{\text{exp}}(x)$ is the experimentally measured elongation of the bonded joint and \bar{h}_A the average thickness of the adhesive layer. An example of the measured stress–strain relationship of the adhesive is shown in Fig. 4.

We can see that this relationship is uniform and nonlinear in the whole strain region $\varepsilon_q(x)$. Such relationship could not easily be expressed using elementary functions. Thus, we introduce the modulus of the adhesive $c_q [\Delta l_q^{\text{exp}}(x)] = \sigma_q(\varepsilon_q)/\varepsilon_q$.

The method for the determination of the modulus c_q is described later in this paper. The function of the force of the adhesive between layers per unit width can be expressed by this modulus as follows [9] (Fig. 11):

$$q(x) = -c_q [\Delta l_q^{\text{exp}}(x)] \Delta l_q^{\text{num}}(x), \quad (2)$$

where $\Delta l_q^{\text{num}}(x) = v_{2L}(x) - v_{1L}(x)$. Using the second-order theory, we can get a system of two differential equations for the equilibrium state of internal bending moments on the deformed layers 1 and 2 in the moment of the local buckling of layer 2. This state will be called state “0” and denoted by a superscript 0. These two differential equations can be written as follows:

$$v_{iL}^{0(IV)}(x) - \omega_{iL}^2 v_{iL}^{0''}(x) + \psi_{iL}^2 \{c_q [\Delta l_q^{\text{exp}}(x)]\} [v_{2L}^0(x) - v_{1L}^0(x)] = 0, \quad i = 1, 2, \quad (3)$$

where $\omega_{iL}^2(x) = N_{iL}^0/D_i(x)$, $\psi_{iL}^2 \{c_q [\Delta l_q^{\text{exp}}(x)]\} = c_q [\Delta l_q^{\text{exp}}(x)]/D_i(x)$, $D_i(x)$ is the flexural rigidity of layer i and N_{iL}^0 is the internal axial force in state “0” in layer i ($i = 1, 2$). The axial forces $N_{iL}^0(x)$ depend on the angles of inclination of the layers, which in state “0” are very small; thus the forces N_{iL}^0 can be considered as constants. The flexural rigidities of the layers are expressed as follows:

$$\begin{aligned} D_1(x) = b \{ & E_1(y_{01}^3 + y_{N1L}^3)/3 + E_1 y_{01} [(h_1 - y_{N1L})^2 - y_{01}^2]/2 \\ & + E_{t1} \{ [(h_1 - y_{N1L})^3 - y_{01}^3]/3 \\ & - y_{01} [(h_1 - y_{N1L})^2 - y_{01}^2]/2 \} \}, \end{aligned} \quad (4)$$

$$\begin{aligned} D_2(x) = b \{ & E_2 [y_{02}^3 - (\delta y_{N2L})^3]/3 + E_2 y_{02} [(h_2 - y_{N2L})^2 - (\delta y_{02})^2]2 \\ & - \delta E_{t2} \{ [(h_2 - y_{N2L})^3 + (\delta y_{02})^3]/3 \\ & + \delta y_{02} [(h_2 - y_{N2L})^2 - (\delta y_{02})^2]2 \} \}, \end{aligned} \quad (5)$$

where $\delta = 1$ for $0 \leq |x| < L_P/2$ and $\delta = -1$ for $L_P/2 < |x| \leq L_0/2$. According to Fig. 2, we can write the following nonhomogeneous boundary conditions:

$$\begin{aligned}
 & 1. \ v_{1L}^0(0) = 0; \quad 2. \ v_{1L}^{0'}(0) = 0; \quad 3. \ v_{2L}^{0'}(0) = 0 \\
 & 4. \ v_{1L}^0(L_0/2) = v_{2L}^0(L_0/2); \quad 5. \ v_{1L}^{0'}(L_0/2) = v_{2L}^{0'}(L_0/2) \\
 & 6. \ M_{1L}^0(L_0/2) = D_1(L_0/2) v_{1L}^{0''}(L_0/2) \\
 & \quad = M_0(1 - b_1/L_1) - M_{BL} - F_0 v_{1L}^0(L_0/2) \\
 & \quad \quad - N_{2BL} [v_{2L}^0(0) - v_{1L}^0(L_0/2)] \\
 & 7. \ M_{2L}^0(L_0/2) = D_2(L_0/2) v_{2L}^{0''}(L_0/2) = -M_{BL} - N_{2BL} [v_{2L}^0(0) - v_{1L}^0(L_0/2)] \\
 & 8. \ Q_{1L}^0(L_0/2) = D_1(L_0/2) v_{1L}^{0'''(L_0/2)} = -(N_{2BL} - F_0) v_{1L}^{0'}(L_0/2).
 \end{aligned} \tag{6}$$

Applying the second-order theory, we can accept the following simplified expression for the shear force $Q_{1L}^0(L_0/2)$ in the boundary conditions (6):

$$Q_{1L}^0(L_0/2) = -(N_{2BL} - F_0) \sin \alpha_{1L}^0(L_0/2) \approx -(N_{2BL} - F_0) v_{1L}^{0'}(L_0/2).$$

The set of equations (3) is nonlinear. An analytical solution would be very difficult to obtain, thus, we will try to get a numerical solution. Using the method of finite differences, we divide the length ($L_0/2$) into $n = 100$ intervals of equal length. In this way, considering the boundary conditions (6), we can transform solving of the set (3) into solving a system of $(2n + 8)$ nonhomogeneous linear equations and solve it numerically by using the Gaussian elimination method [10]. The set of nonlinear equation (3) can be solved successively. In the first step, we choose $c_q [\Delta I_q^{\text{exp}}(x)] = 0$ and determine the deflections $v_{iL}^0(x)$ of the layer i ($i = 1, 2$) and $\Delta I_q^{\text{num}}(x) = v_{2L}(x) - v_{1L}(x)$. From the diagram of $c_q (\Delta I_q^{\text{exp}})$ (Fig. 19), we determine the modulus $c_q (\Delta I_q^{\text{num}})$. The described procedure is repeated until the following condition is fulfilled: $|\Delta I_q^{\text{num}}(j) - \Delta I_q^{\text{num}}(j - 1)| \leq \varepsilon$. The chosen accuracy $\varepsilon = 10^{-5}$ mm is reached after eight steps. Thus, we obtain the bending displacements $v_{iL}^0(x)$ of layer i ($i = 1, 2$) in the domain $0 \leq |x| \leq L_0/2$ in the state "0".

3.2 The force at which an unstable state in layer 2 occurs and the critical external bending moment

In the described model for the determination of the bending displacements of layers in the moment right after local buckling of layer 2, the internal axial force N_{2BL} in layer 2 and the external bending moment M_0 (Fig. 2) are treated as unknowns. Layer 2 buckles locally in the moment at which the compressive axial force in the layer reaches the critical value, N_{2L}^{cr} . Furthermore, it is assumed that layer 2 is bonded to layer 1 with an adhesive whose rigidity is represented by the modulus c_q . The bending moment in layer 2 at point C is $M_{2L}^0(L_0/2) = k v_{2L}^{0'}(L_0/2)$, where k is expressed by the equation: $k = 2 L_1 D_{\text{eq}}(L_0/2) / L_0 (L_1 - L_0)$. Here, the flexural rigidity is

$$\begin{aligned}
 D_{\text{eq}}(x) = b \{ & T_1(x) h_1 [h_1^2 - 3 h_1 y_{NL} + 3 y_{NL}^2] + T_2(x) h_2 [h_2^2 + 3 h_1 (h_1 + h_2) \\
 & - 3 (2 h_1 + h_2) y_{NL} + 3 y_{NL}^2] \} / 3,
 \end{aligned} \tag{7}$$

where $T_i(x) = D_i(x) / I_{zi}$, $I_{zi} = b h_i^3 / 12$ is the second moment of area of layer i ($i = 1, 2$), and $y_{NL} = y_{NL}(x)$ is the distance of the neutral axis from the bottom plane of the plate (Fig. 5).

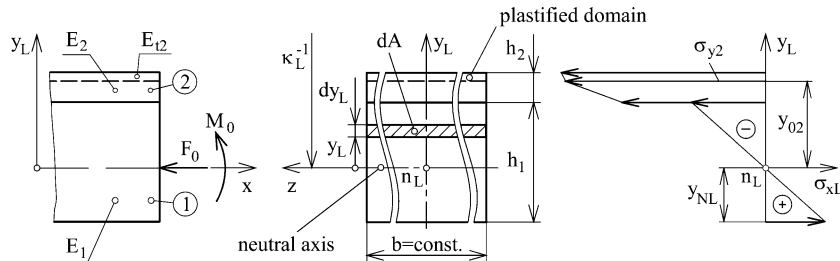


Fig. 5 Normal stress in the plate due to F_0 and M_0

The differential equation of the beam on the foundation is

$$v_{2L}^{0(IV)}(x) + \omega_{2L}^2 v_{2L}^{0''}(x) + \psi_{2L}^2 [c_q (\Delta l_q^{\text{exp}})] v_{2L}^0(x) = 0. \quad (8)$$

It can be solved considering the following homogeneous boundary conditions:

$$\begin{aligned} 1. & \quad v_{2L}^{0'}(0) = 0; \quad 2. \quad v_{2L}^0(L_0/2) = 0 \\ 3. & \quad Q_{2L}^0(0) = D_2(0)v_{2L}^{0'''}(0) = -c_q(0)b v_{2L}^0(0) \\ 4. & \quad M_{2L}^0(L_0/2) = D_2(L_0/2)v_{2L}^{0''}(L_0/2) = k(L_0/2)v_{2L}^0(L_0/2). \end{aligned} \quad (9)$$

By using the QR algorithm [10], we can transform the solving of Eq. (8) into numerical solving of an appropriate eigenvalue problem, and so we get the critical force N_{2L}^{cr} .

The plate is first loaded with a force F_0 that in layer 2 induces an axial force $N_{2L}^{F_0}$, which is smaller than the critical force N_{2L}^{cr} by the aforementioned 10%. The plate is then loaded by an external bending moment M_0^{cr} , due to which an axial force $N_{2L}^{M_0}$ is induced in layer 2, which now buckles locally.

Normal stress in layers 1 and 2 having elastic, linear strain hardening stress–strain relations (Figs. 3 and 5) due to the described loads can be expressed by equation:

$$\begin{aligned} \sigma_{xL}(y_L) &= \sigma_{xL}^{F_0} + \sigma_{xL}^{M_0}(y_L) \\ &= \begin{cases} \frac{N_{1L}^{F_0}}{A_1} - E_1 \kappa_L^{\text{cr}} y_L; & -y_{NL} < y_L \leq h_1 - y_{NL} \\ \frac{N_{2L}^{F_0}}{A_2} - E_2 \kappa_L^{\text{cr}} y_L; & h_1 - y_{NL} \leq y_L < y_{02} \\ \frac{N_{2L}^{F_0}}{A_2} - \sigma_{y2} - E_{t2} \kappa_L^{\text{cr}} (y_L - y_{02}); & y_{02} \leq y_L \leq h_1 + h_2 - y_{NL} \end{cases} \end{aligned} \quad (10)$$

where $N_{iL}^{F_0}$ is the internal axial force in layer i ($i = 1, 2$) due to force F_0 and κ_L^{cr} the curvature of the neutral axis of the plate in the moment of the local buckling. The forces $N_{iL}^{F_0}$ follow from the equilibrium condition for the axial forces $N_{1L}^{F_0} + N_{2L}^{F_0} - F_0 = 0$ (Fig. 2) and from the distribution of the force F_0 to the layers, which is based on the equality condition for the strains of layers due to F_0 [11]: $\varepsilon_{x1L}^{F_0} = \frac{N_{1L}^{F_0}}{A_1 E_1} = \varepsilon_{x2L}^{F_0} = \frac{N_{2L}^{F_0}}{A_2 E_2} - \sigma_{y2} \left(\frac{1}{E_{t2}} - \frac{1}{E_2} \right)$. After some rearrangement, we get the following expressions for the internal axial forces in layers due to F_0 :

$$\begin{aligned} N_{1L}^{F_0} &= \frac{A_1 E_1}{A_1 E_1 + A_2 E_{t2}} \left[F_0 - \sigma_{y2} A_2 E_{t2} \left(\frac{1}{E_{t2}} - \frac{1}{E_2} \right) \right], \\ N_{2L}^{F_0} &= \frac{A_2 E_{t2}}{A_1 E_1 + A_2 E_{t2}} \left[F_0 + \sigma_{y2} A_1 E_1 \left(\frac{1}{E_{t2}} - \frac{1}{E_2} \right) \right]. \end{aligned}$$

On the cross section of the plate loaded with F_0 and M_0 there is a neutral axis where the normal stress (10) is zero (Fig. 5). The position of the neutral axis $y_{NL}(x)$ follows from the equation: $\int_A \sigma_{xL}(y_L) dA = 0$, where A is the cross section of the plate: $A = A_1 + A_2$. The internal axial force $N_{2L}^{M_0}$ due to M_0 is $N_{2L}^{M_0} = N_{2L}^{\text{cr}} - N_{2L}^{F_0}$ and $\kappa_L^{\text{cr}} = M_0^{\text{cr}} [D_{\text{eq}}(L_0/2)]$. After rearrangement, we obtain the critical external bending moment:

$$M_0^{\text{cr}} = \frac{2 D_{\text{eq}}(L_0/2)}{b P_2(L_0/2)} \left(N_{2L}^{\text{cr}} - N_{2L}^{F_0} + \sigma_{y2} A_2 \right), \quad (11)$$

where the flexural rigidity $D_{\text{eq}}(x)$ is determined by Eq. (7), and $P_2(L_0/2)$ is

$$\begin{aligned} P_2(L_0/2) &= E_2 \{ y_{02}^2(L_0/2) - [h_1 - y_{NL}(L_0/2)]^2 \} \\ &\quad + E_{t2} \{ [h_1 + h_2 - y_{NL}(L_0/2)]^2 - y_{02}^2(L_0/2) \}. \end{aligned}$$

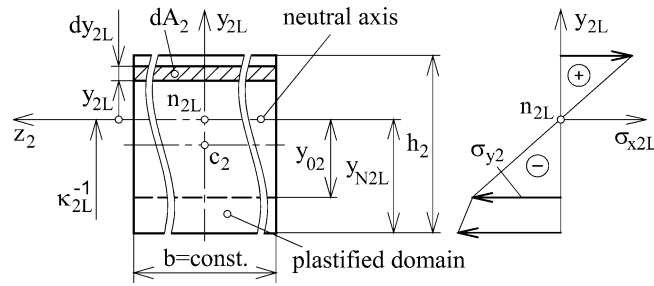


Fig. 7 Normal stress in layer 2 in the domain $0 \leq x < L_P/2$

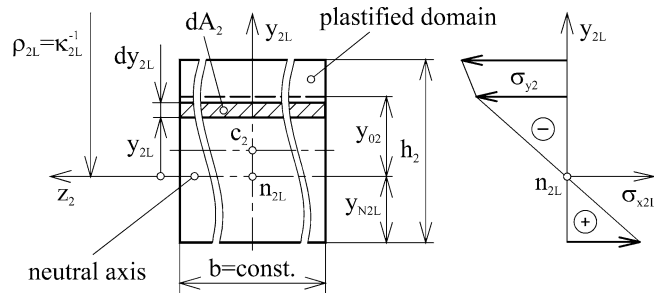


Fig. 8 Normal stress in layer 2 in the domain $L_P < x \leq L_0/2, \kappa_{2L} > 0$

The stress in the domain $0 \leq |x| < L_P/2$ (Fig. 7), considering Eq. (1), is:

$$\begin{aligned} \sigma_{x2L}(y_{2L}) &= \sigma_{x2L}^{F_0} + \sigma_{x2L}^{M_0}(y_{2L}) \\ &= \begin{cases} \frac{\sigma_{y2}}{y_{02}} y_{2L}; & -y_{N2L} \leq y_{2L} \leq -y_{02} \\ -\sigma_{y2} + \frac{E_{t2}}{E_2} \frac{\sigma_{y2}}{y_{02}} (y_{2L} + y_{02}); & -y_{02} < y_{2L} \leq h_2 - y_{N2L} \end{cases} \end{aligned} \quad (15)$$

The stress in the domain $L_P/2 < |x| \leq L_0/2$ (Fig. 8) is also expressed in a similar way:

$$\begin{aligned} \sigma_{x2L}(y_{2L}) &= \sigma_{x2L}^{F_0} + \sigma_{x2L}^{M_0}(y_{2L}) \\ &= \begin{cases} -\frac{\sigma_{y2}}{y_{02}} y_{2L}; & y_{N2L} \leq y_{2L} \leq y_{02} \\ -\sigma_{y2} - \frac{E_{t2}}{E_2} \frac{\sigma_{y2}}{y_{02}} (y_{2L} - y_{02}); & y_{02} < y_{2L} \leq h_2 - y_{N2L} \end{cases} \end{aligned} \quad (16)$$

The depth of the plastified domain of the cross section is: $y_{02}(x) = \sigma_{y2} / [E_2 \kappa_{2L}^0(x)]$. The internal axial force and bending moment can be obtained in a similar way as above for layer 1:

$$\begin{aligned} N_{2L}^0(x) &= b \left\{ \delta \sigma_{y2} [y_{02}^2 - (\delta y_{N2L})^2] / 2 y_{02} - \sigma_{y2} (h_2 - y_{N2L} + \delta y_{02}) (1 - E_{t2} / E_2) \right. \\ &\quad \left. + \delta E_{t2} \kappa_{2L}^0 [(h_2 - y_{N2L})^2 - (\delta y_{02})^2] / 2 \right\} \end{aligned} \quad (17)$$

$$\begin{aligned} M_{2L}^0(x) &= b \left\{ \delta \frac{\sigma_{y2}}{3 y_{02}} [y_{02}^3 - (\delta y_{N2L})^3] - \frac{\sigma_{y2}}{2} [(h_2 - y_{N2L})^2 - (\delta y_{02})^2] \left(1 - \frac{E_{t2}}{E_2} \right) \right. \\ &\quad \left. + \delta E_{t2} \kappa_{2L}^0 [(h_2 - y_{N2L})^3 + (\delta y_{02})^3] / 3 \right\}, \end{aligned} \quad (18)$$

where $\delta = 1$ for $0 \leq |x| < L_P/2$ and $\delta = -1$ for $L_P/2 < |x| \leq L_0/2$. After an increase in the bending moment M_0^{cr} by ΔM_0 at a constant force F_0 , layer 2 reaches the postbuckled state, called state “1” and denoted by superscript 1. Using the third-order theory [9], we can write the following two differential equations for the equilibrium state of internal bending moments on the deformed layers 1 and 2 in state “1”:

$$\kappa_{iL}^{1''}(x) - \omega_{iL}^2 v_{iL}^{1''}(x) + \psi_{iL}^2 \{c_q [\Delta l_q^{\text{exp}}(x)]\} [v_{2L}^1(x) - v_{1L}^1(x)] = 0, \quad i = 1, 2. \quad (19)$$

The curvature $\kappa_{iL}^1(x)$ of layer i in state “1” is:

$$\kappa_{iL}^{1''}(x) = \left[\frac{v_{iL}^{1''}(x)}{\left\{1 + [v_{iL}^{1'}(x)]^2\right\}^{3/2}} \right]'', \quad i = 1, 2, \quad 0 \leq x \leq L_0/2. \quad (20)$$

According to Fig. 2, we can write the following nonhomogeneous boundary conditions:

$$\begin{aligned} & 1. v_{1L}^1(0) = 0; \quad 2. v_{1L}^{1'}(0) = 0; \quad 3. v_{2L}^1(0) = 0 \\ & 4. v_{1L}^1(L_0/2) = v_{2L}^1(L_0/2); \quad 5. v_{1L}^{1'}(L_0/2) = v_{2L}^{1'}(L_0/2) \\ & 6. M_{1L}^1(L_0/2) = D_1(L_0/2) v_{1L}^{1''}(L_0/2) \\ & \quad = M_0(1 - b_1/L_1) - M_{BL} + F_0[v_{TL}^0 - v_{1L}^1(L_0/2)] \\ & \quad \quad - N_{2BL}[v_{2L}^1(0) - v_{1L}^1(L_0/2)] \\ & 7. M_{2L}^1(L_0/2) = D_2(L_0/2) v_{2L}^{1''}(L_0/2) = -M_{BL} - N_{2BL}[v_{2L}^1(0) - v_{2L}^1(L_0/2)] \\ & 8. Q_{1L}^1(L_0/2) = D_1(L_0/2) v_{1L}^{1'''}(L_0/2) = -(N_{2BL} - F_0) \sin \alpha_{1L}^1(L_0/2). \end{aligned} \quad (21)$$

In the boundary condition for $M_{1L}^1(L_0/2)$ in equation (21), we consider the bending deflection v_{TL}^0 in the preceding step of loading, that is, in state “0”. In the j th step of loading, we consider the deflection v_{TL}^{j-1} in the $(j - 1)$ th step of loading.

Using the method of finite differences, we transform the solving of the set of equations (19), considering the boundary conditions (21), into solving a system of $(2n + 8)$ nonhomogeneous nonlinear equations. We solve it numerically by using the modified Powell’s algorithm [12]. As the initial bending displacements we use those which were determined in state “0”: $v_{1L}^0(x)$ and $v_{2L}^0(x)$. Thus, we obtain the bending displacements $v_{iL}^1(x)$ and curvatures $\kappa_{iL}^1(x)$ of layer i ($i = 1, 2$) in the domain $0 \leq |x| \leq L_0/2$ in state “1”. The internal axial forces and bending moments follow from Eqs. (13), (14), (17) and (18) with the replacement of the superscript “0” with “1”. The described procedure is repeated during the entire process of increasing bending moment M_0 by ΔM_0 at a constant force F_0 .

3.4 Bonded part of the plate—Phases 1 and 2

If the plate is cut through in the bonded domain in the very vicinity of point C (Fig. 9), the domain C–T can be treated as a cantilever beam bonded of two layers having certain mechanical properties. We can replace the influence of the left part cut off on its right by the external force F_0 and the bending moments M_{CL} and M_{TL} .

For the equilibrium state of internal bending moment, we can obtain a differential equation for the determination of the bending displacements of the bonded part:

$$\kappa_L''(x) + \omega_L^2 [v_{CL}''(x) + v_L''(x)] = 0, \quad (22)$$

where $\kappa_L(x)$ is the curvature of the bonded part and $\omega_L^2 = F_0/[D_{eq}(L_0/2)]$. The second derivative of $\kappa_L(x)$ is determined by Eq. (20) and the flexural rigidity $D_{eq}(x)$ by Eq. (7). Considering the nonhomogeneous boundary

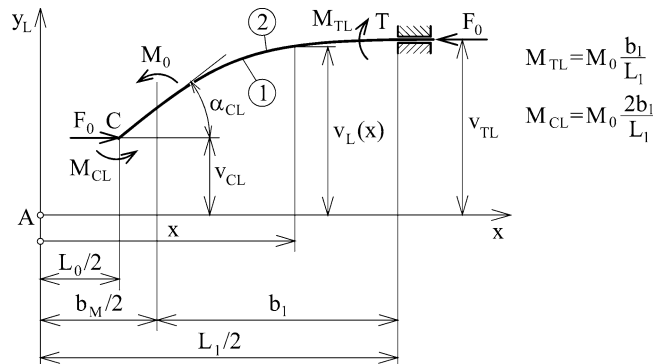


Fig. 9 Bonded part of the plate

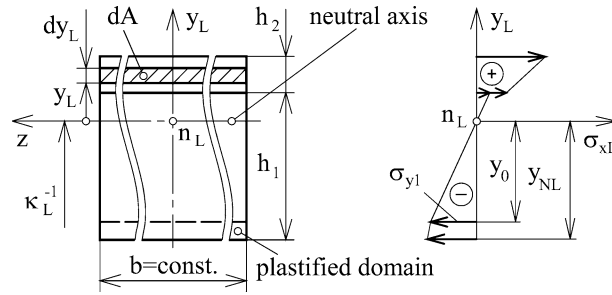


Fig. 10 Normal stress in the bonded part of the plate

conditions (Fig. 9)

$$\begin{aligned} 1. \quad v_L(L_0/2) &= v_{CL}; & 3. \quad v'_L(L_1/2) &= 0 \\ 2. \quad v'_L(L_0/2) &= \tan \alpha_{CL}; & 4. \quad v''_L(L_0/2) &= v''_{CL} = M_{CL}/[D_{eq}(L_0/2)] \end{aligned} \quad (23)$$

and by using the method of finite differences, we transform the solving of the differential equation (22) into numerical solving of a system of $(n + 4)$ nonlinear equations. This is solved in the way described above with $n = 100$ intervals. Thus we obtain the bending displacements $v_L(x)$ of the bonded part in all states during the entire process of increasing the external loading.

Considering the stress–strain relations (1) of both layers and according to Fig. 10, we can determine the normal stress in the bonded part due to the loading with the axial force and bending moment:

$$\sigma_{xL}(y_L) = \begin{cases} -\sigma_{y1} + \frac{E_{t1}}{E_1} \frac{\sigma_{y1}}{y_0} (y_0 + y_L); & -y_{NL} \leq y_L < -y_0 \\ \frac{\sigma_{y1}}{y_0} y_L; & -y_0 \leq y_L \leq h_1 - y_{NL} \\ \frac{E_2}{E_1} \frac{\sigma_{y1}}{y_0} y_L; & h_1 - y_{NL} \leq y_L \leq h_1 + h_2 - y_{NL} \end{cases} \quad (24)$$

From the way of loading and chosen materials of both layers it is shown that plastification first takes place in layer 1. Therefore, the depth of the plastified domain can be determined in the point between the elastic and plastic domain of the cross section of layer 1: $y_0(x) = \sigma_{y1}/[E_1 \kappa_L(x)]$. The internal axial force and bending moment follow from the equilibrium conditions, considering Eq. (24):

$$\begin{aligned} N_L(x) &= - \int_A \sigma_{xL}(y_L) dA(y_L) \\ &= -b \sigma_{y1} \left\{ (y_{NL} - y_0) + \frac{E_{t1}}{E_1} \frac{1}{y_0} \left[y_0 (y_0 - y_{NL}) - \frac{1}{2} (y_0^2 - y_{NL}^2) \right] \right. \\ &\quad \left. - \frac{1}{2y_0} [(h_1 - y_{NL})^2 - y_0^2] - \frac{E_2}{E_1} \frac{h_2}{2y_0} [h_2 + 2(h_1 - y_{NL})] \right\} \end{aligned} \quad (25)$$

$$\begin{aligned} M_L(x) &= - \int_A \sigma_{xL}(y_L) y_L dA(y_L) \\ &= -b \sigma_{y1} \left\{ \frac{1}{2} (y_0^2 - y_{NL}^2) - \frac{E_{t1}}{E_1} \frac{1}{y_0} \left[\frac{y_0}{2} (y_0^2 - y_{NL}^2) + \frac{1}{3} (y_{NL}^3 - y_0^3) \right] \right. \\ &\quad \left. - \frac{1}{3y_0} [(h_1 - y_{NL})^3 + y_0^3] \right. \\ &\quad \left. - \frac{E_2}{E_1} \frac{1}{3y_0} [(h_1 + h_2 - y_{NL})^3 - (h_1 - y_{NL})^3] \right\} \end{aligned} \quad (26)$$

3.5 Mechanism of growth of the debonded area

In the initial phase of the process, external loads are small and strains in both layers are equal. When the external loads increase, the stress and strain in the adhesive increase too. At the moment of local buckling of

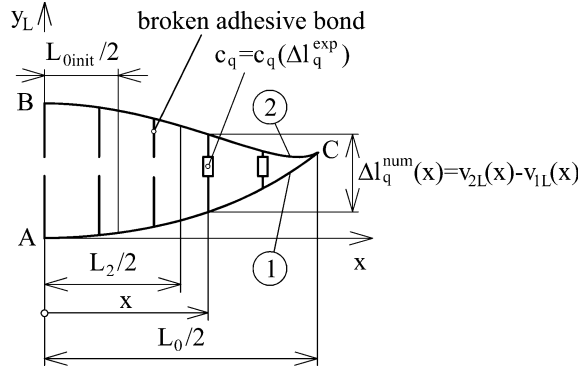


Fig. 11 The length L_{0init} of the initially debonded area, the length L_2 over which adhesive bonds are torn apart and the length L_0 of the debonded area

layer 2, the adhesive bonds between layers 1 and 2 can break at the weakest spot. This can occur due to the presence of the initially debonded area of length L_{0init} (Fig. 11). The plate in the debonded area splits into two subsystems. The main subsystem is represented by layer 1, which at increasing external loads bends, while the weaker layer 2 is the locally buckled layer. On the remaining part the plate remains bonded.

In the postbuckled state, the bending displacement states of the layers and the strains of adhesive bonds change due to the increasing external bending moment $M_0 > M_0^{cr}$. These changes, considering the stress–strain relation of the adhesive, result in an increase in the tensile stress in the adhesive. When this stress exceeds a certain critical value, the adhesive bonds tear apart over domain $L_2 < L_0$ (Fig. 11). In the domain $(L_0 - L_2)$ the adhesive bonds are extended but not yet torn. Length L_2 (Fig. 11) is defined on the basis of a limit strain ε_{qlim} of the adhesive at a limit stress $\sigma_{qlim} = 0.1\sigma_{qmax}$ (Fig. 4), where σ_{qmax} is the maximal tensile stress in the adhesive. In each state with increasing M_0 , the following equilibrium condition in the bonding layer, with respect to point C, is fulfilled: $M_{qint}(L_0) - M_{qext}(M_0) = 0$, where $M_{qint}(L_0)$ is the internal bending moment due to the rigidity of the adhesive bonds, and $M_{qext}(M_0)$ the external bending moment which results in tearing of the adhesive bonds. These moments are as follows:

$$M_{qint}(L_0) = b \int_{L_2/2}^{L_0/2} c_q [\Delta l_q^{exp}(x)] \left(\frac{L_0}{2} - x \right) dx;$$

$$M_{qext}(M_0) = (v_{BL} - v_{CL}) N_{2BL}(M_0), \quad (27)$$

where v_{BL} and v_{CL} are the bending displacements of layer 2 at points B and C, respectively, and $N_{2BL}(M_0)$ is the internal axial force in layer 2 at point B (Fig. 2).

The moment M_{qext} increases with the increasing M_0 . The equilibrium of the moments M_{qext} and M_{qint} during an increasing M_0 can be fulfilled if the length L_0 of the debonded area also increases. The length L_0 reaches a maximal value $L_0 = L_{0max}$ at a certain limit value M_{0lim} of the external bending moment. At this moment, in the vicinity of point C in the debonded domain, a compressive stress in the bonding layer appears, stopping any further growth of the debonded area. The maximal length L_{0max} can be calculated from the equilibrium condition: $M_{qint}(L_{0max}) - M_{qext}(M_{0lim}) = 0$, where $M_{qint}(L_{0max})$ and $M_{qext}(M_{0lim})$ are obtained from Eq. (27). On further increasing $M_0 > M_{0lim}$, the length L_{0max} remains unchanged.

3.6 The state after unloading of the plate—Phase 3

The process of unloading the plate ($M_0 \rightarrow 0$, $F_0 \rightarrow 0$) is completed within a very short period. During this process, stresses in both layers decrease linearly with respect to strains. The cross section of layer 1 was partially plastified during the loading ($M_0 \neq 0$, $F_0 \neq 0$). This is why after unloading layers it does not return into the same undeformed state as prior to loading. At the moment of unloading, due to a ruined equilibrium state, internal axial forces and internal bending moments in the layers appeared in the opposite direction to that during loading.

After unloading has been completed, the equilibrium state in the plate is restored. The following relationships exist between the internal forces and bending moments in layers 1 and 2 in the debonded part of the plate

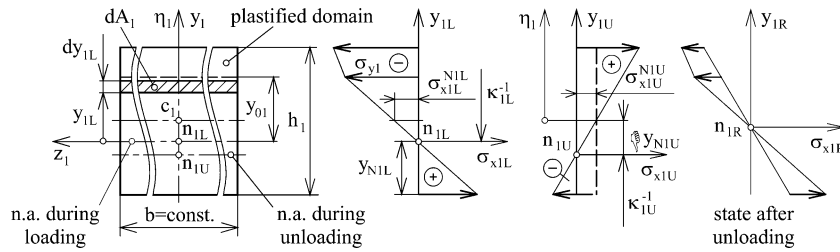


Fig. 12 Normal stresses in layer 1 in all three phases of the process

in all three phases of the process, that is, during the process of loading, during the process of unloading and in the state after unloading:

$$\begin{aligned} N_{iR}(x) &= N_{iL}(x) + N_{iU}(x), & Q_{iR}(x) &= Q_{iL}(x) + Q_{iU}(x) \\ M_{iR}(x) &= M_{iL}(x) + M_{iU}(x), & i &= 1, 2, \quad 0 \leq |x| \leq L_0/2. \end{aligned} \quad (28)$$

The bending displacement states of layers 1 and 2 in the debonded part of the plate in all phases of the process must satisfy the following conditions [13]:

$$v_{iR}(x) = v_{iL}(x) + v_{iU}(x), \quad i = 1, 2, \quad 0 \leq |x| \leq L_0/2, \quad (29)$$

or in terms of curvatures:

$$\kappa_{iR}(x) = \kappa_{iL}(x) + \kappa_{iU}(x), \quad i = 1, 2, \quad 0 \leq |x| \leq L_0/2. \quad (30)$$

In layer 1 (Fig. 12), the process of unloading follows a straight line in the σ - ε diagram. The neutral axis during unloading coincides with the centroid c_1 of the cross section and thus the curvature κ_{1U} during unloading is:

$$\kappa_{1U}(x) = \frac{-\varepsilon_{x1U}^{M1U}(x)}{\eta_1(x)} = \frac{-\sigma_{x1U}^{M1U}(\eta_1)}{[E_1 \eta_1(x)]}, \quad (31)$$

where $\eta_1 = \eta_1(x)$ is the distance from the centroid (Fig. 12).

The bending stress $\sigma_{x1U}^{M1U}(\eta_1)$ during unloading can be obtained by introducing Eq. (31) into Eq. (30) and considering the following relationship between the coordinates η_1 , y_{1U} and Δy_{N1U} (Fig. 12): $\eta_1(x) = y_{1U}(x) - \Delta y_{N1U}(x)$. After some rearrangement, we get:

$$\sigma_{x1U}^{M1U}(y_{1U}) = (y_{1U} - \Delta y_{N1U}) (\sigma_{y1}/y_{01} - E_1 \kappa_{1R}). \quad (32)$$

The stress σ_{x1U}^{N1U} due to the axial force N_{1U} during unloading can be expressed by the force N_{1U} and the cross section A_1 . From Fig. 12 we can also see that between the stress σ_{x1U}^{N1U} , the curvature κ_{1U} and the distance Δy_{N1U} , the following relationship exists: $\sigma_{x1U}^{N1U} = -E_1 \kappa_{1U} \Delta y_{N1U}$. Introducing Eqs. (31) and (32) and expression for $\eta_1(x)$ into the mentioned relationship, we get:

$$\sigma_{x1U}^{N1U} = N_{1U}/A_1 = \text{const.} = -E_1 \kappa_{1U} \Delta y_{N1U} = \Delta y_{N1U} (\sigma_{y1}/y_{01} - E_1 \kappa_{1R}). \quad (33)$$

The stress during the unloading is the sum of Eqs. (32) and (33):

$$\sigma_{x1U}(y_{1U}) = \sigma_{x1U}^{N1U}(y_{1U}) + \sigma_{x1U}^{M1U}(y_{1U}) = y_{1U} (\sigma_{y1}/y_{01} - E_1 \kappa_{1R}). \quad (34)$$

The axial force during unloading can be obtained from the equilibrium condition in the cross section of the layer for internal axial forces:

$$N_{1U} = - \int_{A_1} \sigma_{x1U}(y_{1U}) dA_1(y_{1U}) = -b h_1 \Delta y_{N1U} (\sigma_{y1}/y_{01} - E_1 \kappa_{1R}), \quad (35)$$

where is $dA_1(y_{1U}) = bdy_{1U}$. The internal bending moment during unloading acts at the centroid and follows from the equilibrium condition in the cross section of the layer for bending moments:

$$\begin{aligned} M_{1U} &= - \int_{A_1} \sigma_{x1U}(y_{1U}) y_{1U} dA_1(y_{1U}) \\ &= -b h_1 (\sigma_{y1}/y_{01} - E_1 \kappa_{1R}) (h_1^2 + 12 \Delta y_{N1U}^2)/12. \end{aligned} \quad (36)$$

By introducing Eqs. (13), (14), (35) and (36) into Eq. (28), we get the resulting internal axial force and bending moment in layer 1 in the state after unloading:

$$\begin{aligned} N_{1R} &= N_{1L} + N_{1U} \quad \text{for } 0 \leq |x| \leq L_0/2 \\ N_{1R} &= -b \left\{ \frac{\sigma_{y1}}{2y_{01}} (y_{01}^2 - y_{N1L}^2) + \sigma_{y1} (h_1 - y_{N1L} - y_{01}) \left(1 - \frac{E_{t1}}{E_1} \right) \right. \\ &\quad \left. + \frac{E_{t1} \kappa_{1L}}{2} [(h_1 - y_{N1L})^2 - y_{01}^2] \right\} - b h_1 \Delta y_{N1U} \left(\frac{\sigma_{y1}}{y_{01}} - E_1 \kappa_{1R} \right) \end{aligned} \quad (37)$$

$$\begin{aligned} M_{1R} &= M_{1L} + M_{1U} \quad \text{for } 0 \leq |x| \leq L_0/2 \\ M_{1R} &= -b \left\{ \frac{\sigma_{y1}}{3y_{01}} (y_{01}^3 + y_{N1L}^3) + \frac{\sigma_{y1}}{2} [(h_1 - y_{N1L})^2 - y_{01}^2] \left(1 - \frac{E_{t1}}{E_1} \right) \right. \\ &\quad \left. + \frac{E_{t1} \kappa_{1L}}{3} [(h_1 - y_{N1L})^3 - y_{01}^3] \right\} \\ &\quad - \frac{b h_1}{12} \left(\frac{\sigma_{y1}}{y_{01}} - E_1 \kappa_{1R} \right) (h_1^2 + 12 \Delta y_{N1U}^2). \end{aligned} \quad (38)$$

The process of unloading of layer 2 also follows a straight line in the σ - ε diagram. Since the bending displacement curve of layer 2 has the inflection point $|x| = L_P/2$ (Fig. 2), the unloading is treated in two separate domains. Fig. 13 shows the stresses in the domain $0 \leq |x| < L_P/2$ in all three phases of the process, while Fig. 14 shows the stresses in the domain $L_P/2 < |x| \leq L_0/2$.

The resulting internal axial force and bending moment in the state after unloading can be expressed in a similar way as above for layer 1:

$$\begin{aligned} N_{2R} &= N_{2L} + N_{2U} \\ N_{2R} &= b \left\{ \delta \frac{\sigma_{y2}}{2y_{02}} [y_{02}^2 - (\delta y_{N2L})^2] - \sigma_{y2} (h_2 - y_{N2L} + \delta y_{02}) \left(1 - \frac{E_{t2}}{E_2} \right) \right. \\ &\quad \left. + \delta \frac{E_{t2} \kappa_{2L}}{2} [(h_2 - y_{N2L})^2 - (\delta y_{02})^2] \right\} \\ &\quad + \delta b h_2 \Delta y_{N2U} \left(\frac{\sigma_{y2}}{y_{02}} - E_2 \kappa_{2R} \right) \end{aligned} \quad (39)$$

$$\begin{aligned} M_{2R} &= M_{2L} + M_{2U} \\ M_{2R} &= b \left\{ \delta \frac{\sigma_{y2}}{3y_{02}} [y_{02}^3 - (\delta y_{N2L})^3] - \frac{\sigma_{y2}}{2} [(h_2 - y_{N2L})^2 - (\delta y_{02})^2] \left(1 - \frac{E_{t2}}{E_2} \right) \right. \\ &\quad \left. + \delta \frac{E_{t2} \kappa_{2L}}{3} [(h_2 - y_{N2L})^3 + (\delta y_{02})^3] \right\} \\ &\quad - \frac{b h_2}{12} \left(\frac{\sigma_{y2}}{y_{02}} - E_2 \kappa_{2R} \right) (h_2^2 + 12 \Delta y_{02U}^2), \end{aligned} \quad (40)$$

where $\delta=1$ for $0 \leq |x| < L_P/2$ and $\delta = -1$ for $L_P/2 < |x| \leq L_0/2$.

The unloading of the bonded part of the plate also reaches completion in the elastic stress domain of both layers (Fig. 15). After the process of unloading has been completed, the equilibrium state in the bonded part is restored.

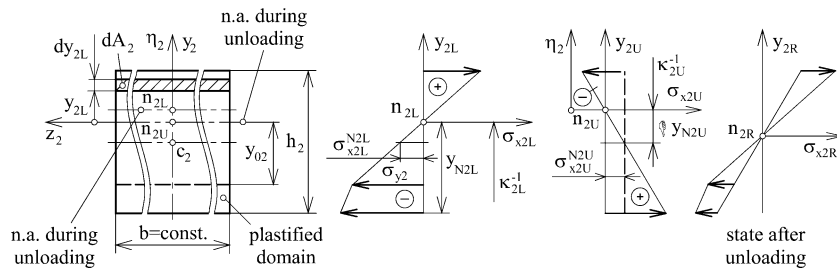


Fig. 13 Normal stresses in layer 2 in the domain $0 \leq x < L_p/2$ in all three phases of the process

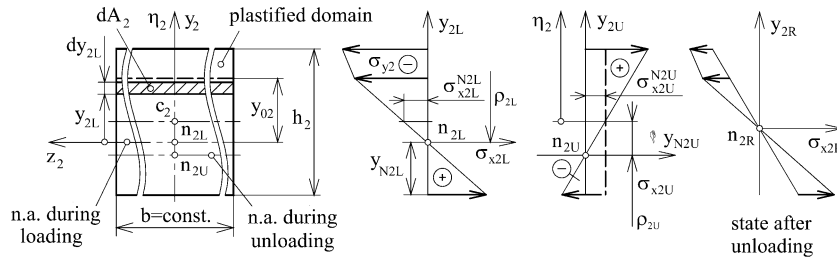


Fig. 14 Normal stresses in layer 2 in the domain $L_p/2 < x \leq L_0/2$ in all three phases of the process

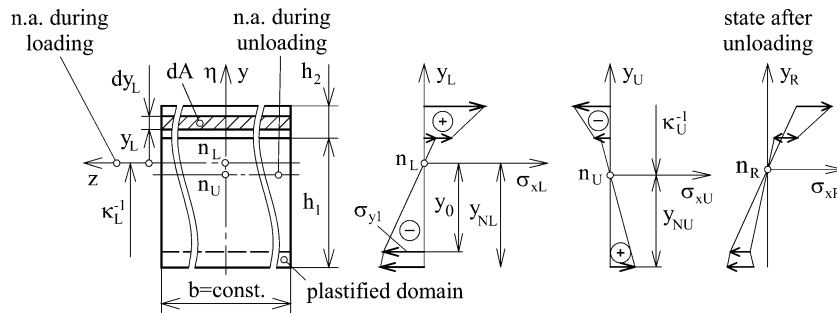


Fig. 15 Normal stresses in the bonded part of the plate in all three phases of the process

The following relationships exist between the internal forces and bending moments in the bonded part during loading, unloading and in the state after unloading:

$$\begin{aligned} N_R(x) &= N_L(x) + N_U(x), & Q_R(x) &= Q_L(x) + Q_U(x) \\ M_R(x) &= M_L(x) + M_U(x), & L_0/2 \leq |x| \leq L_1/2. \end{aligned} \quad (41)$$

The bending displacements and curvatures in all phases of the process must satisfy the following condition [13]:

$$v_R(x) = v_L(x) + v_U(x), \quad \kappa_R(x) = \kappa_L(x) + \kappa_U(x), \quad L_0/2 \leq |x| \leq L_1/2. \quad (42)$$

The curvature κ_U during unloading refers to the neutral axis n_U during unloading and has the opposite sign to that during loading. It can be expressed by the coordinate $\eta(x)$:

$$\kappa_U(x) = \frac{-\sigma_{x1U}^{M_U}(\eta)}{E_1 \eta(x)}. \quad (43)$$

The bending stress $\sigma_{x1U}^{M_U}(\eta)$ in layer 1 of the bonded part during unloading can be obtained by introducing Eq. (43) into Eq. (42) and considering the relationship between the coordinates η and y_U (Fig. 15): $\Delta y_{NU}(x) = \eta(x) - y_U(x)$. We also consider the relationship between the bending stresses in the layers during

unloading: $\sigma_{x2U}^{M_U}/\sigma_{x1U}^{M_U} = E_2/E_1$. After rearrangement, we get:

$$\begin{aligned}\sigma_{x1U}^{M_U}(y_U) &= (y_U + \Delta y_{NU}) (\sigma_{y1}/y_{01} - E_1 \kappa_R); \\ \sigma_{x2U}^{M_U}(y_U) &= E_2/E_1 \sigma_{x1U}^{M_U}(y_U)\end{aligned}\quad (44)$$

The stresses in the layers due to the axial force during unloading follow by considering the relations: $\sigma_{x1U}^{N_U} = N_U/A_1 = -M_U \Delta y_{NU}/I_{z1} = \text{constant}$, and $\sigma_{x2U}^{N_U}/\sigma_{x1U}^{N_U} = E_2/E_1$:

$$\begin{aligned}\sigma_{x1U}^{N_U}(y_U) &= -\Delta y_{NU} (\sigma_{y1}/y_{01} - E_1 \kappa_R); \\ \sigma_{x2U}^{N_U}(y_U) &= -E_2/E_1 \sigma_{x1U}^{N_U}(y_U).\end{aligned}\quad (45)$$

The normal stress in the bonded part during unloading is the sum of Eqs. (44) and (45):

$$\sigma_{xU}(y_U) = y_U \left(\frac{\sigma_{y1}}{y_0} - E_1 \kappa_R \right) \begin{cases} 1; & -y_{NU} \leq y_U \leq h_1 - y_{NU} \\ E_2/E_1; & h_1 - y_{NU} \leq y_U \leq h_1 + h_2 - y_{NU} \end{cases}\quad (46)$$

The internal axial force and bending moment in the bonded part during unloading can be obtained from the equilibrium condition for the axial forces and bending moments:

$$\begin{aligned}N_U &= - \int_A \sigma_{xU}(y_U) dA(y_U) \\ &= b [E_1 h_1 (h_1 - 2y_{NU}) + E_2 (2h_1 + h_2 - 2y_{NU})] \\ &\quad \times [\kappa_R - \sigma_{y1}/(E_1 y_0)]/2\end{aligned}\quad (47)$$

$$\begin{aligned}M_U &= - \int_A \sigma_{xU}(y_U) y_U dA(y_U) \\ &= \frac{b}{2} \left\{ \frac{E_2}{E_1} [(h_1 + h_2 - y_{NU})^3 - (h_1 - y_{NU})^3] + (h_1 - y_{NU})^3 - y_{NU}^3 \right\} \\ &\quad \times \left(E_1 \kappa_R - \frac{\sigma_{y1}}{y_0} \right),\end{aligned}\quad (48)$$

where $dA(y_U) = b dy_U$. The resulting internal axial force and bending moment after unloading follow by introducing Eqs. (25), (26), (47) and (48) into Eq. (41):

$$\begin{aligned}N_R &= N_L + N_U \quad \text{for } L_0/2 \leq |x| \leq L_1/2 \\ N_R &= -b \sigma_{y1} \left\{ (y_{NL} - y_0) + \frac{E_{t1}}{E_1} \frac{1}{y_0} \left[y_0 (y_0 - y_{NL}) - \frac{1}{2} (y_0^2 - y_{NL}^2) \right] \right. \\ &\quad \left. - \frac{1}{2 y_0} [(h_1 - y_{NL})^2 - y_0^2] - \frac{E_2}{E_1} \frac{h_2}{2 y_0} [h_2 + 2 (h_1 - y_{NL})] \right\} \\ &\quad + \frac{b}{2} [E_1 h_1 (h_1 - 2y_{NU}) + E_2 (2h_1 + h_2 - 2y_{NU})] \left(\kappa_R - \frac{\sigma_{y1}}{E_1 y_0} \right)\end{aligned}\quad (49)$$

$$\begin{aligned}M_R &= M_L(x) + M_U(x) \quad \text{for } L_0/2 \leq |x| \leq L_1/2 \\ M_R &= -b \sigma_{y1} \left\{ \frac{1}{2} (y_0^2 - y_{NL}^2) - \frac{E_{t1}}{E_1} \frac{1}{y_0} \left[\frac{y_0}{2} (y_0^2 - y_{NU}^2) + \frac{1}{3} (y_{NL}^3 - y_0^3) \right] \right. \\ &\quad \left. - \frac{1}{3 y_0} [(h_1 - y_{NL})^3 + y_0^3] - \frac{E_2}{E_1} \frac{1}{3 y_0} [(h_1 + h_2 - y_N)^3 - (h_1 - y_{NL})^3] \right\} \\ &\quad + \frac{b}{2} \left\{ \frac{E_2}{E_1} [(h_1 + h_2 - y_{NU})^3 - (h_1 - y_{NU})^3] + (h_1 - y_{NU})^3 - y_{NU}^3 \right\} \\ &\quad \times \left(E_1 \kappa_R - \frac{\sigma_{y1}}{y_0} \right).\end{aligned}\quad (50)$$

4 Experimental work

For experimental evaluation of the mathematical model, we chose a bonded two-layer plate-strip. The layers are made of isotropic materials, while the bonding material is Neoprene adhesive having a certain rheological model. Experimental work was performed using a Zwick Z050 electronic measurement device (EMD) equipped with Multisens extensometers, nominal force 50 kN, crosshead travel resolution of $0.5 \mu\text{m}$ and measurement range error 0.5% from 1/50 of the nominal force. The EMD makes it possible to load test pieces in a combined way with tensile and compressive axial forces. In our experimental work, we first determined the mechanical properties of the chosen materials of the layers and adhesive, and then experimentally verified the mathematical model.

4.1 Mechanical properties of chosen materials

According to the standard [14], tensile tests were performed in order to measure the mechanical properties of materials of the plate-strip layers. For the thicker layer, we chose Peral AlMg3, Impol Slovenska Bistrica, Slovenia. For the weaker layer, we chose cold-reduced grain-oriented transformer steel Unisil-M 103-27P, Orb Electrical Steel Ltd., Newport, South Wales, UK. The selection of the mentioned materials was based on the observations during tensile tests, which showed that the stress–strain relationships of both materials were elastic, linear and strain hardening (Fig. 16).

The following mechanical properties in the tensile stress domain were determined: Young's modulus E in the elastic domain, yield stress σ_y , strain ε_y at the yield stress and tangent modulus E_t in the plastic domain, see Table 1. We estimate that the measured mechanical properties of both materials can also be accepted in the compressive stress domain.

For bonding the layers, Neoprene adhesive Neostik SK-101, Belinka Kemostik, Slovenia, was chosen. According to the standard [15], the stress–strain relationship of the adhesive was measured on the series of 25 test pieces bonded from steel and Peral, see Fig.17.

Test pieces were loaded with the increasing tensile force F . The criterion for stopping the test was a prescribed limit elongation of the bonded joint $\Delta l_q^{\text{exp}} = 3 \text{ mm}$ at which adhesive bonds were to be torn apart. The measured stress–strain relationships are shown in Fig.19.

Using the definition $c_q [\Delta l_q^{\text{exp}}(x)] = \sigma_q(\varepsilon_q) / \varepsilon_q$, we tabulated the average modulus of the adhesive $c_q [\Delta l_q^{\text{exp}}(x)]$ with respect to the experimentally measured elongation $\Delta l_q^{\text{exp}}(x)$ (Fig.19 right). The strain of the bonded joint is defined by equation $\varepsilon_q(x) = \Delta l_q^{\text{exp}}(x) / \bar{h}_A$, where $\bar{h}_A = 0.077 \text{ mm}$ is the average thickness of the adhesive layer. The modulus c_q in the singular point $\Delta l_q^{\text{exp}} = 0$ was calculated by interpolating the tabulated values. The mechanical properties of the materials of the layers and the average modulus c_q were used as inputs to compute the bending displacements of layers.

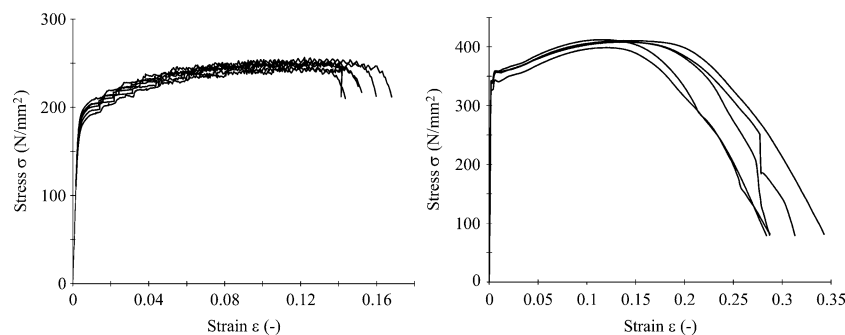


Fig. 16 Measured stress–strain relations for Peral AlMg3 (*left*) and Unisil-M 103-27P (*right*)

Table 1 Average values of mechanical properties of the materials of layers 1 and 2

Material	E (N/mm ²)	σ_y (N/mm ²)	ε_y	E_t (N/mm ²)
Peral AlMg3	0.656×10^5	188.12	4.37×10^{-3}	0.62×10^4
Unisil-M 103-27P steel	2.048×10^5	337.33	3.6×10^{-3}	1×10^4

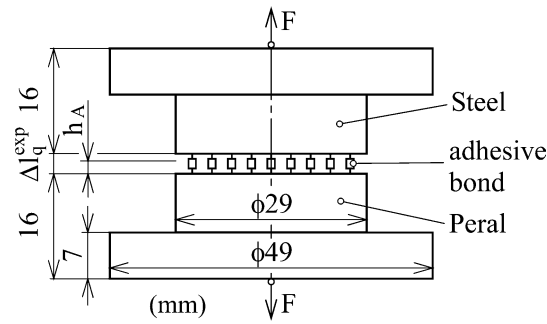


Fig. 17 Standard test piece for determination of stress-strain relationship of the adhesive [15]

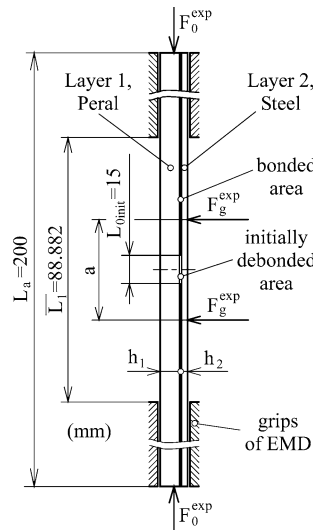


Fig. 18 Principle of compressive-bending experiment

4.2 Experimental verification of the mathematical model

Compressive-bending experiments were performed in order to see how the presented mathematical model suited the real conditions. We chose a rigidly fixed plate-strip of width $b = 10$ mm. The average length of test pieces was $\bar{L}_1 = 88.882$ mm (Fig.18). The thickness of the layer made of Peral AlMg3 was $h_1 = 2$ mm and the thickness of the weaker layer made of Unisil-M 103-27P steel was $h_2 = 0.27$ mm. A symmetrical initial debonding was caused over a length $L_{0init} = 15$ mm (Fig.18) by inserting a $d = 0.19$ mm thick wire into the plate (Fig.21).

Due to the vertical orientation of the workplace, it would be very difficult to exert the bending load using a couple of bending moments in the way proposed in the mathematical model. A bending load with a couple of shear forces F_g^{exp} was applied to the test pieces, which was made possible by a specially designed device that was mounted onto the EMD. The method of determination of the forces F_g^{exp} and distance a is explained in Fig.20. In case **a**, the beam is loaded with bending moment M_0 , while in case **b** with a couple of forces F_g^{exp} . From the diagrams of bending moments in Fig.20, we can see that the described ways of bending loads are not comparable with each other.

To obtain correct experimental results in the region of maximal length of debonded area the following three conditions must be fulfilled:

1. The distance b_M between the external moments M_0 must be much larger than the maximal length of the debonded area L_{0max} of the beam;
2. The maximal bending displacements v_D of the beam at point D in cases a and b must be equal;

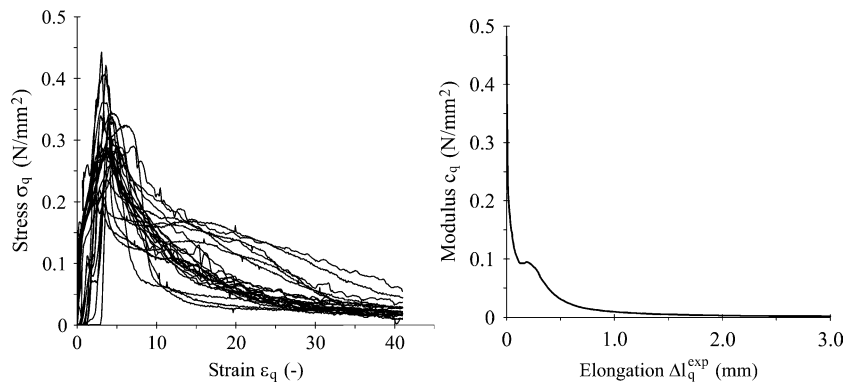


Fig. 19 Measured stress–strain relationships (*left*) and average modulus c_q of the chosen adhesive with respect to elongation Δl_q^{exp} (*right*)

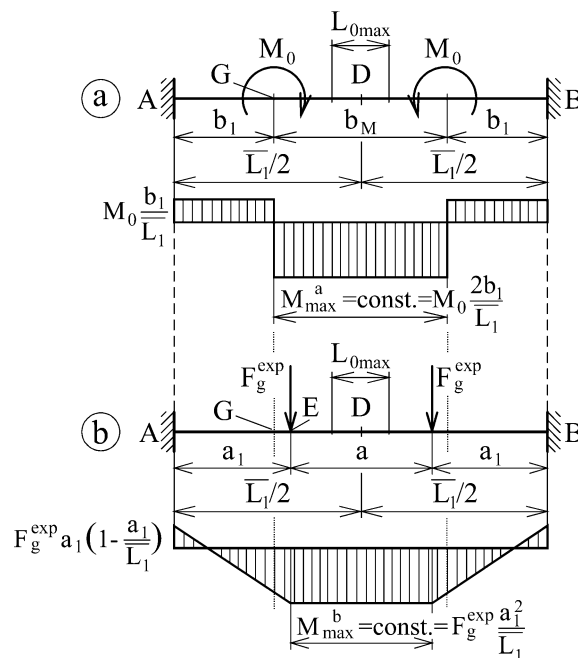


Fig. 20 Method of determination of the shear force F_g^{exp}

3. The maximal internal bending moment at the same point D in cases a and b must be equal. The force F_g^{exp} and distance a are as follows:

$$F_g^{\text{exp}} = 2M_0 \frac{b_1}{a_1^2}; \quad a = \frac{(3b_M - \bar{L}_1)}{2}. \quad (51)$$

The internal bending moments over the length $a > L_{0\text{max}}$ in both cases a and b are constant and equal: $M_{\text{max}}^a = M_{\text{max}}^b = M_{\text{max}}$. The differences between the bending displacements and relative differences between internal bending moments at points G, E and D in both cases a and b are as follows:

$$\begin{aligned} \Delta v_G &= v_G^a - v_G^b = -3.867 M_0 / (E I_z); & (M_G^a - M_G^b) / M_{\text{max}} &= -0.1711 \\ \Delta v_E &= v_E^a - v_E^b = 1.294 \cdot 10^{-3} M_0 / (E I_z); & (M_E^a - M_E^b) / M_{\text{max}} &= 0 \\ \Delta v_D &= v_D^a - v_D^b = 0; & (M_D^a - M_D^b) / M_{\text{max}} &= 0, \end{aligned} \quad (52)$$

where $I_z = bh^3/12$ is the second moment of area, b is the width, h is the thickness of the beam, E is the Young's modulus, v_i^a and v_i^b are the bending displacements at point i , $i = G, E, D$ in case a and b, respectively. Before

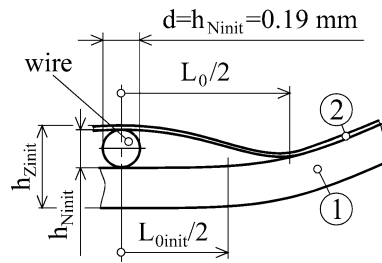


Fig. 21 Method of measurement of the external height h_Z and length L_0 of the debonded area

loading, a wire of diameter d was inserted between the layers on the initially debonded area of length L_{0init} (Fig. 21). The diameter d was equal to the previously calculated initial internal height h_{Ninit} of the debonded area right after local buckling (state “0”).

Using a couple of weights F_g^{exp} acting on the distance a , the bending load was applied to the test pieces. The plate-strip was then loaded by increasing the compressive axial force F_0^{exp} . After the axial force had reached the critical value $F_0^{exp} = F_{01}^{exp}$, the weaker layer entered the postbuckled state (state “1”). Bending displacements of the layers exceeded the initial value $d = h_{Ninit} = 0.19$ mm. We measured the compressive axial forces F_{01}^{exp} in the mentioned state “1”. The axial force F_0 was further increasing at a constant shear force F_g^{exp} until it reached the prescribed value $F_{02}^{exp} = -685$ N (state “2”). We measured the external height h_{Z2}^{exp} and length L_{02}^{exp} of the debonded area. The force F_0 was further increasing at a constant force F_g^{exp} until it reached the prescribed maximal value $F_{03}^{exp} = F_{0max}^{exp}$ (Fig.22).

In this state, called state “3”, we measured the external height h_{Z3}^{exp} and length L_{03}^{exp} . As the criterion for stopping the loading, we chose the axial compressive force F_{0max}^{exp} that had previously been numerically determined. In the state after unloading (state “4”), we measured the external height h_{Z4}^{exp} and length L_{04}^{exp} .

The experiments were performed using 17 test pieces. Based on the measured results, we calculated the average values of the length \bar{L}_1 , critical force \bar{F}_{01}^{exp} for local buckling, external height \bar{h}_Z^{exp} and length \bar{L}_0^{exp} of the debonded area, see Table 2.

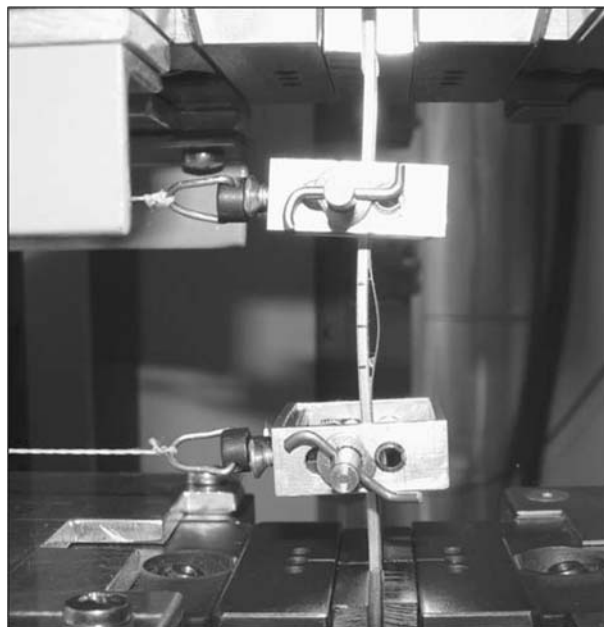


Fig. 22 State “3” at maximal axial force F_{0max}^{exp} at a constant shear force F_g^{exp}

Table 2 Average values of the measured results of compressive-bending experiments

State “0”	State “1”	State “2”	State “3”	State “4”
\bar{L}_1 (mm)	$\bar{F}_{01}^{\text{exp}}$ (N)	$\bar{h}_{Z2}^{\text{exp}}$ (mm)	$\bar{L}_{02}^{\text{exp}}$ (mm)	$\bar{h}_{Z3}^{\text{exp}}$ (mm)
88.882	-438.824	2.793	17.059	3.424
				$\bar{L}_{03}^{\text{exp}}$ (mm)
				20.353
				$\bar{h}_{Z4}^{\text{exp}}$ (mm)
				2.715

5 Numerical example

Based on the presented mathematical model a computer program was developed. It enables the determination of the critical force $N_{2L_{\text{cr}}}^{\text{num}}$ and critical external moment $M_{0\text{cr}}^{\text{num}}$ at which the weaker layer buckles locally, the computation of the displacement states of the layers in the moment after local buckling, during increasing external loading and in the state after unloading. A numerical example was set up to see how the physical model corresponded to the real conditions. A rigidly fixed plate-strip of width $b = 10$ mm, thickness of layer 1, $h_1 = 2$ mm, and thickness of layer 2, $h_2 = 0.27$ mm, was chosen. Other dimensions were as shown in Fig.18. The average values of the measured mechanical properties of the layers (Table 1), the modulus of the adhesive c_q (ΔJ_q^{exp}) and the length of $L_{0\text{init}} = 15$ mm over which the layers were initially debonded were considered. Based on a chosen distance b_M and length L_1 , the distance $a = 45.559$ mm (Fig.20) was calculated.

The loading model was chosen so that the axial force F_0 performed 90% of the compressive force for local buckling of layer 2 while the remaining part was contributed by the bending moment M_0 . This is in accordance with the assumption made in the mathematical model. In the moment of local buckling of layer 2 the following values were computed: critical force for local buckling: $N_{2L_{\text{cr}}}^{\text{num}} = -588.04$ N; critical axial force: $F_{0\text{cr}}^{\text{num}} = N_{2L_{\text{cr}}}^{\text{num}}/0.9 = -653.38$ N; critical bending moment: $M_{0\text{cr}}^{\text{num}} = 304.14$ N mm; the necessary weight: $F_{g\text{cr}}^{\text{num}} = 24.525$ N; internal and external height of debonded area: $h_{N\text{init}} = 0.19$ mm and $h_{Z1}^{\text{num}} = 1.325$ mm; initial length of debonded area: $L_{0\text{init}} = 15$ mm.

The bending displacements $v(x)$ in the following states of the loading process and in the state after unloading were computed, see Fig.23:

- State “1”: Loading with $F_{01}^{\text{exp}} = F_{0\text{cr}}^{\text{num}} = -653.38$ N and $F_g^{\text{exp}} = 24.525$ N.
- State “2”: Loading with $F_{02}^{\text{exp}} = -685$ N at a constant value $F_g^{\text{exp}} = 24.525$ N.
- State “3”: Loading with $F_{03}^{\text{exp}} = -1433$ N at a constant value $F_g^{\text{exp}} = 24.525$ N.
- State “4”: State after unloading: $F_{04}^{\text{exp}} = 0$, $F_g^{\text{exp}} = 0$.

From Fig. 23, we can see that the bending displacements increase with increasing axial force F_0^{exp} at a constant weight F_g^{exp} . The bending displacements of the bonded part of the plate-strip during increasing F_0^{exp} (states “1”, “2” and “3”) were determined with an assumed rigid support of the plate-strip at point T, Fig. 2. After unloading, i.e. in state “4”, the plate-strip flattens. Due to stresses in the elasto-plastic domain in state “3”, the tangent to the bonded part of the plate-strip at the same point T is no longer parallel to the x -axis, Fig. 23.

Figure 24 presents the length L_0^{num} of the debonded area with respect to the bending moment M_0^{num} at a constant force $F_{03}^{\text{exp}} = -1433$ N. The length of the debonded area suddenly increases from $L_{0\text{init}} = 15.0$ mm to $L_0^{\text{num}} = 16.6$ mm at a constant bending moment $M_{0\text{cr}}^{\text{num}} = 304.14$ N mm. This is a consequence of using the second-order theory. The length L_0 then increases with increasing bending moment and reaches its maximal value $L_{0\text{max}}^{\text{num}} = 20.6$ mm at the maximal bending moment $M_{0\text{max}}^{\text{num}} = 404.54$ N mm. After unloading of the plate-strip, the length $L_{0\text{max}}^{\text{num}}$ remains unchanged.

6 Discussion

The physical adequacy of the presented mathematical model was evaluated by comparing the numerically and experimentally obtained results for the external height h_Z and length L_0 of the debonded area. The experimentally obtained results in the three states of loading and in the state after unloading were compared by determining relative differences with respect to numerically obtained values. Table 3 shows the relative differences $e_{h_{Zi}}$ between the experimentally and numerically obtained results for external height h_Z , where $i = 1, 2, 3, 4$ is the number of the state. Table 4 shows the relative differences $e_{L_{0i}}$ between the experimentally and numerically obtained results for the length L_0 .

From Table 3, we can see that the maximal relative difference in the external height h_Z occurs in state “3”. The relative difference $e_{h_{Z1}}$ in state “2” is -1.1% and in state “4” is -4.5% , whereas the relative differences

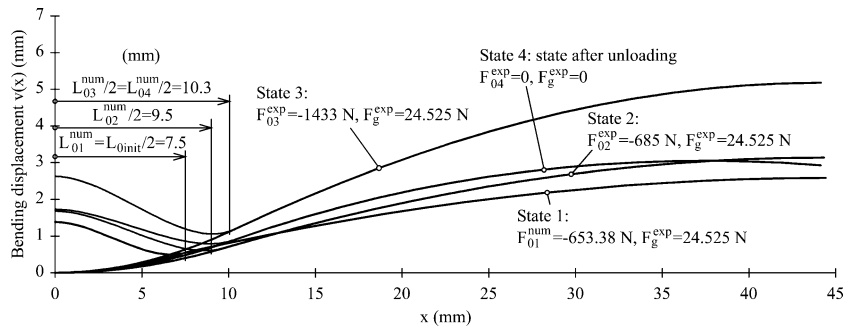


Fig. 23 Bending displacement states of plate-strip in the four states of the process

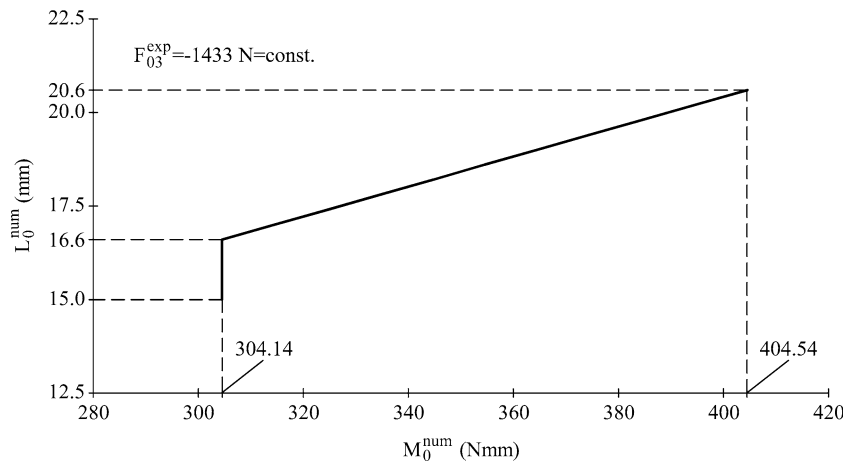


Fig. 24 Debonded length L_0^{num} with respect to the external bending moment M_0^{num}

e_{L_0} in states “3” and “4” are the same, i.e. -1.2% (Table 4). These tables show very good agreement between the results obtained in both ways. This is, in our opinion, thanks to the use of the third-order theory in the development of the mathematical model for the determination of the displacement states of the plate. In the numerical example, the measured mechanical properties of the chosen materials of layers and adhesive were considered.

All experimentally obtained results are slightly below the numerically obtained ones, which shows the presence of certain nonidealities. We estimate that the existing differences between the results obtained in both ways can be explained by the assumptions made in the mathematical model, which were the following:

1. The plate was taken to be ideally flat prior to loading.
2. In the numerical model, average mechanical properties of materials were considered. During measurement of mechanical properties of the adhesive a certain scatter of results was observed, which is shown in the description of the experimental work.
3. In the mathematical model, the bending load was considered to be performed by a couple of bending moments while in the experiments, the bending load was performed by a couple of shear forces.

7 Conclusions

The problem of local buckling of the weaker layer of a two-layer plate loaded with external compressive force and bending moment is treated. The conditions for the growth of the debonded area in the plate have been studied. On the basis of the experiments it can be concluded that the axial force should be slightly lower than the buckling force of the weaker layer. Instability and the local buckling process can appear when an additional bending moment is applied to the plate. The numerical model also confirms this. To see how the presented mathematical model suited the real conditions, a numerical example has been set up in which experimentally obtained results were considered.

Table 3 Comparison of experimentally and numerically obtained height h_Z (mm)

State "1"		State "2"		State "3"		State "4"	
$\bar{h}_{Z1}^{\text{exp}}$	h_{Z1}^{num}	$\bar{h}_{Z2}^{\text{exp}}$	h_{Z2}^{num}	$\bar{h}_{Z3}^{\text{exp}}$	h_{Z3}^{num}	$\bar{h}_{Z4}^{\text{exp}}$	h_{Z4}^{num}
1.325	1.325	2.793	2.825	3.424	3.746	2.715	2.843
e_{hZ1} (%)	0	e_{hZ2} (%)	-1.1	e_{hZ3} (%)	-8.6	e_{hZ4} (%)	-4.5

Table 4 Comparison of experimentally and numerically obtained length L_0 (mm)

State "1"		State "2"		State "3"		State "4"	
$\bar{L}_{01}^{\text{exp}}$	L_{01}^{num}	$\bar{L}_{02}^{\text{exp}}$	L_{02}^{num}	$\bar{L}_{03}^{\text{exp}}$	L_{03}^{num}	$\bar{L}_{04}^{\text{exp}}$	L_{04}^{num}
15.00	15.00	17.06	19.0	20.353	20.6	20.353	20.6
e_{L01} (%)	0	e_{L02} (%)	-10.2	e_{L03} (%)	-1.2	e_{L04} (%)	-1.2

The main subsystem bends due to the proposed external loads, while the remaining subsystem buckles locally into a shape for which a minimal potential energy is needed. This shape is symmetric with respect to the symmetric axis of the debonded area. Both subsystems remain bonded over a certain domain. From the graphs it is shown that the length of the debonded area increases with increasing bending moment at a constant axial force up to a certain limit value.

The physical adequacy of the mathematical model is evaluated by a comparison of experimentally and numerically obtained results for the external height and length of the debonded area. The mentioned results were compared in the three states of loading process and in the unloaded state by determining the relative differences with respect to numerically obtained values. The maximum difference between the results for the length of the debonded area is -10.2% . The maximum difference for the external height of the debonded area is -8.6% . From these values it can be concluded that results obtained from the two methods are in sufficient agreement.

References

1. Whitcomb, J.D.: Mechanics of instability-related delamination growth. In: Garbo, S.P. (ed.) Composite materials: testing and design, vol 9. ASTM STP 1059. American Society for Testing and Materials, Philadelphia pp. 215–230 (1990)
2. Kardomateas, G.A.: The initial post-buckling and growth behavior of internal delaminations in composite plates. *Trans ASME J Appl Mech* **60**, 903–910 (1993)
3. Simitses, G.J., Sallam, S., Yin, W.L.: Effect of delamination on axially loaded homogeneous laminated plates. *AIAA J* **23**, 1437–1444 (1985)
4. Chai, H.: Three-dimensional analysis of thin film debonding. *Int J Fracture* **46**, 237–256 (1990)
5. Whitcomb, J.D.: Finite element analysis of instability related delamination growth. *J Comp Mat* **15**, 403–426 (1981)
6. Bruno, D., Grimaldi, A.: Delamination failure of layered composite plates loaded in compression. *Int J Sol Struct* **26**, 313–330 (1990)
7. Koselj, F., Kuselj, B., Batista, M.: Delamination of two-layer plate-strip. In: Proceedings of the third international conference design to manufacture in modern industry, 8–9 September. Portorož (1997)
8. Kuselj, B., Koselj, F.: The growth of debonded area in a bonded two-layer plate-strip. *Zangew Math Mech* **81**(Suppl 2), 313–314 (2001)
9. Timoshenko, S.P., Gere, J.M.: Theory of elastic stability, 2nd edn. McGraw-Hill, New York (1961)
10. Gerald, C.F., Wheatley, P.O.: Applied numerical analysis, 6th edn. Addison Wesley/Longman, Reading/London (1999)
11. Gere, J.M.: Mechanics of materials, 5th edn. Brooks/Cole, Pacific Grove (2001)
12. IMSL.: Fortran subroutines for mathematical applications, Visual Numerics (1997)
13. Koselj, F., Borštnik, I.: Bending of the beams of constant cross-section in the elasto-plastic domain. *J Mech Eng* **9–10** 205–208 (1979)
14. DIN EN 10002.: Metallic materials; tensile testing; Part 1: method of testing (at ambient temperature). German Version EN 10002–1: 1990 + AC1:1990 (1990)
15. ASTM D 897-95a.: Standard test method for tensile properties of bonded joints. American Society for Testing and Materials, Philadelphia (1995)